Originally published as:

High-resolution image of the geometry and thickness of the subducting Nazca lithosphere beneath northern Chile

F. Sodoudi,[1] X. Yuan,[1] G. Asch,[1] and R. Kind[1]

[1]   Results obtained from *S* and *P* receiver functions produced a clear image of the top and bottom of the subducting Nazca lithosphere beneath northern Chile. Using data from the teleseismic events recorded at 15 permanent Integrated Plate Boundary Observatory Chile (IPOC) stations, we obtained new constraints on the geometry and thickness of the descending Nazca lithosphere. We observed the subducted crust of the Nazca plate at depths ranging from 50 km beneath the Coastal Cordillera down to 110 km beneath the Western Cordillera. We found significant along-strike variations in the geometry of the Nazca plate beneath northern Chile. On closer inspection, it appears that the oceanic Nazca plate is divided into two distinct segments as it descends beneath the continental South American plate. The transition from the relatively steeper (~23°) and deeper slab to the north of 21°S to the flatter southern segment (~19°) is shown reasonably clearly by our data. This feature could well be associated with variations in the curvature of the plate margin and the geometry of the Chile trench, which is mainly curved to the north of 21°S. We have also mapped the continental Moho of the South American plate at depths ranging between 60 and 70 km to the east of the Longitudinal Valley. Beneath the Coastal Cordillera, this boundary becomes invisible, probably due to the serpentinization of the forearc mantle wedge that reduces the velocity in the uppermost mantle. The base of the subducted Nazca plate was clearly identified as a sharp boundary in the results obtained from the *P* and *S* receiver functions. The thickness of the subducted oceanic Nazca plate, which has an age of ~50 My, is estimated to be ~50 km. Although this thickness is consistent with that predicted by thermal gradients, the explanation of the sharpness of the lithosphere-asthenosphere boundary may require another mechanism such as hydration or melting.

1. Introduction

[2] The concept of mobile lithospheric plates that move over a weaker asthenosphere is the fundamental premise of plate tectonics. The determination of the thickness of the lithospheric plates is therefore one of the most essential issues in the understanding of global tectonics. Newly created oceanic lithosphere cools, subsides and thickens as it spreads away from mid-ocean ridges. It is reheated on returning to the mantle at subduction zones. The resulting thermal evolution of the oceanic lithosphere governs its properties as a function of age [*Stein and Stein*, 1992]. The subduction of the oceanic Nazca plate beneath the continental South American plate belongs to long-lived subduction systems [*Gurnis et al.*, 2004], which periodically generates massive earthquakes. The Chile trench has been subject to the subduction and migration of several spreading ridges along its margin [*Sdrolias and Müller*, 2006]. These processes have significantly altered the shape, structure and dip of the subducting slab. The present-day age of the subducting Nazca lithosphere ranges from 0 My at the intersection with the Nazca-Antarctic ridge, to 50 My at latitude 20°S [*Sdrolias and Müller*, 2006]. The forearc of the Chilean Andes therefore offers an unparalleled opportunity to study the processes that affect the leading edge of a continent-ocean convergent plate boundary.

[3] A large number of focused geophysical investigations has made the Nazca subduction zone one of the best known convergent margins on Earth [e.g., *Beck et al.*, 1996; *Bock et al.*, 2000; *Buske et al.*, 2002; *Giese et al.*, 1999; *Götze et al.*, 1994; *Haberland and Rietbrock*, 2001; *Husen et al.*, 1999; *Khazaradze and Klotz*, 2003; *Oncken et al.*, 1999, 2003; *Patzwahl et al.*, 1999; *Schurr et al.*, 2003, 2006; *Wigger et al.*, 1994; *Yuan et al.*, 2000]. The geometry of the Nazca subduction zone has also been largely constrained by the spatial distribution of the earthquake hypocenters [*Barazangi and Isacks*, 1976; *Bevis and Isacks*, 1984; *Cahill and Isacks*, 1992; *Comte and Suárez*, 1995]. These studies have pro-

[1]Helmholtz Centre Potsdam, GFZ German Research Centre for Geosciences, Potsdam, Germany.
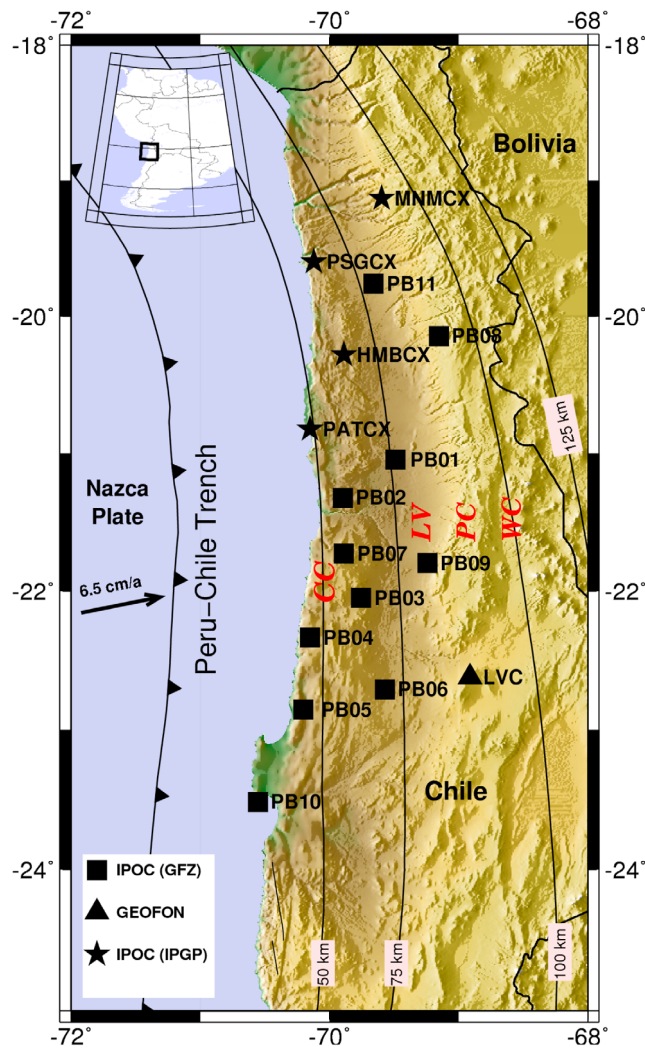
Figure 1. Topographical map of the central Andes including major tectonic features and seismic stations. The black squares and stars are the IPOC permanent broadband stations operated since 2006 by GFZ Potsdam and IPGP Paris, respectively. We also used data from one GEOFON (black triangle) station located in northern Chile. The black lines indicate the contours of the Wadati-Benioff zone [*Cahill and Isacks*, 1992]. CC, Coastal Cordillera; LV, Longitudinal Valley; PC, Precordillera; WC, Western Cordillera. The arrow indicates the direction of relative motion between the Nazca and South American plates [*Angermann et al.*, 1999].

vided valuable information on the processes of subduction, and yielded significant constraints on the nature of the crustal and intracrustal structures, but none of them has been successful in mapping the lithosphere-asthenosphere boundary (LAB). The thickness of the subducting Nazca lithosphere is a matter that has therefore remained largely unresolved.

[4] The thickness of the lithosphere and the rheological contrasts between the lithosphere and asthenosphere are expressed in a variety of seismological studies. Observations of seismic surface waves reveal a well-developed zone where seismic wave velocities are low beneath the ocean basins, at depths of about 80–200 km [e.g., *Cammarano and Romanowicz*, 2007; *Kustowski et al.*, 2008]. It is likely that

this low-velocity zone corresponds to the low-viscosity asthenosphere. However, with this technique, the LAB cannot be imaged with sufficient resolution in both the lateral and vertical directions. Wide-angle body wave data from natural or controlled source experiments have a higher resolution, but no sufficiently dense observations are available. A seismic technique that makes use of converted waves (*P*-to-*S* and *S*-to-*P*) has now been developed far enough to be useful in observations of the LAB with a sufficiently high resolution and density [e.g., *Abt et al.*, 2010; *Geissler et al.*, 2010; *Heit et al.*, 2007; *Kawakatsu et al.*, 2009; *Rychert and Shearer*, 2009; *Sodoudi et al.*, 2006a, 2006b, 2009]. A growing number of regional observations obtained from *P* and *S* receiver function studies has found evidence for discontinuities characterized by a significant negative velocity contrast in the upper mantle [*Fischer et al.*, 2010] and provided new constraints on the physical and chemical properties that differentiate the lithosphere from the asthenosphere. Conversions from an LAB-like discontinuity have also clearly been observed in oceanic regions. These phases generally indicate a large and rapid LAB velocity gradient and are consistent with an anomalously hot asthenosphere that is rich in water or contains partial melt. The existence of *S*-to-*P* and *P*-to-*S* phases from an oceanic LAB showed that the LAB velocity gradient is relatively sharp beneath ocean. Recent *P* and *S* receiver function studies on relatively unperturbed oceanic lithosphere [e.g., *Kawakatsu et al.*, 2009; *Rychert and Shearer*, 2009] indicated a sharp LAB with a velocity drop of 7–8% over less than 10–15 km. In many cases, resulting discontinuities can be also compared with shear wave velocity models from surface-wave tomography [e.g., *Rychert and Shearer*, 2009; *Abt et al.*, 2010]. Significant energy from *S*-to-*P* converted waves at the LAB beneath the South American plate was recently detected by *Heit et al.* [2007]. They observed a relatively sharp LAB down to depths of 220 km, which they interpreted as the LAB of the subducted oceanic Nazca plate. This boundary could not be previously resolved by surface wave study in central and western South America [*van der Lee et al.*, 2001].

[5] Establishment of the Integrated Plate Boundary Observatory Chile (IPOC) began in 2006 in close collaboration with Universidad de Chile (Santiago), Universidad Catolica del Norte (Antofagasta), IPGP (Paris), and GFZ Potsdam, with the aim of improving our understanding of the physical processes of earthquakes and of the deformation at the continental margin of Chile. Currently more than 15 modern seismological stations are operated in northern Chile. The data obtained from the dense IPOC network has allowed the resolution of geological characteristics more clearly than has previously been possible, and has provided detailed constraints on the shape and thickness of the descending Nazca lithosphere beneath northern Chile.

[6] We herein focus on the region of northern Chile that lies between latitudes 19°S and 24°S, an area that is approximately bounded to the west by the Coastal Cordillera (CC), and to the east by the western rim of the volcanic arc that forms the Western Cordillera (Figure 1). We use two different methods (*P* and *S* receiver functions) to obtain a high-resolution image of the subducting Nazca lithosphere. The *P* receiver function method is used to resolve the most prominent structures beneath the station, while the *S* receiver

Table 1. Stations and Their Geographical Coordinates

Station	Latitude (deg)	Longitude (deg)	Altitude (m)
PB01	−21.04	−69.48	900
PB02	−21.31	−69.89	1015
PB03	−22.04	−69.75	1460
PB04	−22.33	−70.14	1520
PB05	−22.85	−70.2	1150
PB06	−22.7	−69.57	1440
PB07	−21.72	−69.88	1570
PB08	−20.14	−69.15	3060
PB09	−21.79	−69.24	1530
PB10	−23.51	−70.55	250
PB11	−19.75	−69.65	1300
MMCX	−19.13	−69.59	2304
PSGCX	−19.59	−70.12	966
HMBCX	−20.27	−69.88	1152
PATCX	−20.82	−70.15	832
LVC	−22.61	−68.91	2915

function method is especially useful in determining the LAB. A combination of these two analyses herein provides a clear image of the subducted mantle lithosphere of the Nazca plate for the first time.

2. Data and Methodology

[7] Teleseismic data were recorded using 15 permanent IPOC stations (Figure 1 and Table 1) and were used to calculate the *P* and *S* receiver functions. We added to our data set by using records obtained from a GEOFON station (LVC) located in northern Chile (Table 1). All stations were equipped with STS-2 broadband seismometers. More than three years of data were available for most of the stations. All teleseismic events at a distance of 30°–95° that had a magnitude (mb) greater than 5.5 were analyzed for *P* receiver functions. We computed *P* receiver functions for all stations in a manner as described by *Yuan et al.* [1997]. We rotated the ZNE component waveforms into the local LQT ray-based coordinate system and deconvolved the L component from the Q component to isolate the *P*-to-*S* conversions on the Q component. The rotation angles (back azimuth and incidence angle) were determined by the eigenvalues of the covariance matrix over a time window spanning the first few seconds following the *P* wave arrival. For the *S* receiver functions, due to the lack of the events at a distance range of 60°–85°, we used the SKS phases of earthquakes with magnitudes greater than 5.7 (mb) that occurred at epicentral distances of 85°–115°. We selected the angle of incidence by minimizing the *S* wave energy on the L component and rotated the three component ground motion into the ray coordinate system of L, Q and T [see also *Kumar et al.*, 2006]. Deconvolution of the Q component from the L component results in having the converted *S*-to-*P* phases on the L component. To make the *S* receiver functions directly comparable with the *P* receiver functions, we reverse the time axis and the polarities of the *S* receiver functions [see also *Sodoudi et al.*, 2006b]. We corrected the moveout of both the *P* and *S* receiver functions using the same reference slowness of 6.4 s/deg, and stacked the receiver functions according either to the station locations or the piercing points. We converted the arrival times to depths using migration according to the IASP91 reference model [*Kennett and Engdahl*, 1991].

[8] There are different sources of errors in the *P* and *S* receiver function analysis. The velocity model (IASP91), which is used to perform the time to depth conversion may introduce an error of 3 km in the Moho depth and 5 km in the LAB depth, if we assume that the seismic velocity varies in the crust by up to 5%. The dominant wave periods of the *P* and *S* waves (~1 s and ~4 s, respectively) may theoretically result in a maximum depth resolution of 1 km for *P*-to-*S* and 6 km for *S*-to-*P* conversions. Lateral heterogeneities and noise may also add some more errors. Therefore the errors introduced into depth estimates of Moho and slab (Moho of the oceanic plate) are roughly estimated to be less than 5 km (using *P* receiver functions), whereas the errors in the LAB depths determined by *S* receiver functions are about 10 km.

3. Observations

[9] More than 80 *P* receiver functions (PRFs) obtained from a single station (PB03) are shown in Figure 2. They are filtered using a low-pass filter of 1 s and sorted by back azimuth. The most pronounced positive phase, which is strongly imaged at about 8 s, is related to the Moho of the subducting Nazca plate (labeled S). Another positive phase at a delay time of about 3 s is interpreted as an intracrustal layer (labeled C). The conversion from the Moho of the South American plate cannot be significantly resolved by our data. *Yuan et al.* [2002] observed the Moho at 4 s delay time by stacking receiver functions from many stations in this area. This phase seems to be visible in some of our individual receiver functions (at 4.5 s). A weak converted phase with negative amplitude at about 12 s indicates a decreasing velocity with depth (labeled L), and may give some indication of the presence of the LAB of the subducted oceanic plate.

[10] The *S* receiver functions (SRFs) were also calculated for each station. Since the locations of *S*-to-*P* piercing points were further away from the stations, we divided the whole area into 31 boxes related to the distribution of the *S*-to-*P* conversions (Figure 3a) at a depth of 100 km (the approximate depth of the LAB). Conversion points are calculated using the IASP91 reference model. The size of each box approximately corresponds to the number of SRFs that cross it. We summed the SRFs within each box. Figure 3b shows all the SRFs located within box I4, after they had been filtered using a low-pass filter of 4 s. Besides the strong phases marked C (at 3 s) and S (at 10 s), which are conversions from the intracrustal structure and the Moho of the subducting Nazca plate (slab), there is another pronounced phase with negative amplitude at about 16 s. This phase is likely related to the LAB (labeled L).

4. Results and Discussion

[11] We stacked the PRFs obtained from all stations in bins of 0.05° and sorted them according to the longitude of their piercing points at a depth of 100 km (Figure 4a). The most pronounced conversions correspond to the Moho of the subducting Nazca plate (shown as slab), which is clearly shown at times ranging from 4 s beneath the offshore region and Coastal Cordillera to about 11 s beneath the Western Cordillera. The probable *P*-to-*S* converted phases associated

SODOUDI ET AL.: SUBDUCTING NAZCA LITHOSPHERE
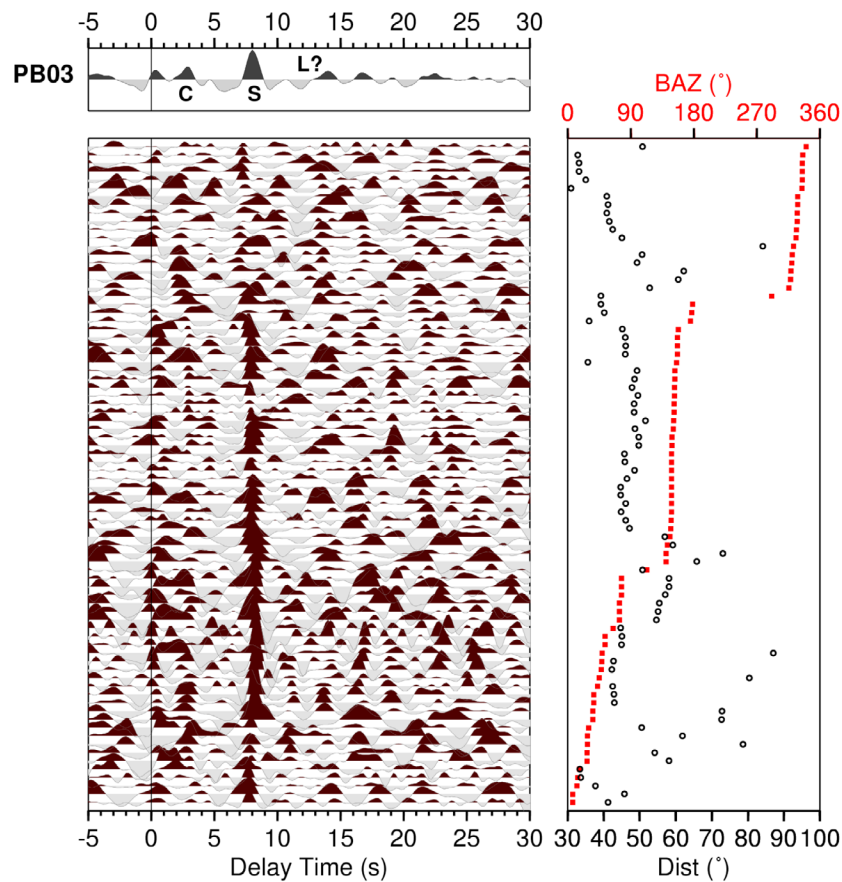
Figure 2. Single PRFs with summation trace for station PB03. Individual moveout-corrected PRFs are equally spaced and sorted by back azimuth (shown with red rectangles). They are filtered using a low-pass filter of 1 s. Black dots indicate the epicentral distances. The converted phases from the intracrustal structure (marked with C) and the Moho of the subducated plate (marked with S) are well observed. A weak conversion with a negative polarity (at 12 s) may indicate conversion at the LAB of the subducted Nazca plate (marked with L).

with the LAB (shown as LAB) are also visible in some parts of the profile. However, we observed a strong depth scattering of the slab phase (e.g., at longitudes −70.3°, −69.3° and −69.5°). In Figure 4b we show the PRFs stacked at each station and sorted by longitude. A significant oscillation of the arrival times of the slab phases is clearly visible. This phenomenon may be explained by the along-strike variation in the subduction geometry found beneath northern Chile. It seems likely that the subducting Nazca plate has two different segments (marked with dashed lines in Figure 4b); the southern segment (in red, marked with 1) can be only identified in the PRFs of the stations located to the south of 21°S. In the same way, the PRFs of the stations located to the north of 21°S show the northern segment of the Nazca plate (in blue, marked with 2), which is deeper and steeper than the southern segment. Latitude 21°S seems to represent a boundary that separates these two parts of the slab. This result may also be confirmed by the Wadati-Benioff Zone depth contours shown by *Cahill and Isacks* [1992]. The eastward bend of the 100 km depth contour of seismicity at 22°S is consistent with the gently slipping segment to the south (see also Figure 1). Evidence for a trench-perpendicular tear in the subducting Nazca plate at 21°S

was also reported by *Rietbrock and Haberland* [2002]. Using temporary data obtained from a local seismic network, they suggested that a segment of the Nazca plate was being pushed downward to the north of 21°S. *Comte and Suárez* [1995] estimated the geometry of the subducting Nazca plate using joint hypocentral determination from teleseismic earthquakes. They observed a gradual southward flattening of the slab in northern Chile, and suggested that the change from a steep to a more subhorizontal mode of subduction could occur at about 21°S.

[12] More detailed images of the geometry of the subducted Nazca plate may be obtained from our migrated PRF data. Figure 5 shows two profiles derived from the depth migration of PRFs for the northern and southern parts of the region, respectively. Along latitude 20°S (data bands of 1° at each side of the profile), the PRFs clearly show the existence of two different plates (Figure 5a). The Moho of the continental South American plate is well seen beneath the eastern part of the profile up to the east of the Coastal Cordillera (labeled Moho). A thick crust of about 70 km is clearly imaged beneath the Western Cordillera. The crust becomes thinner and is approximately 60 km thick beneath the Precordillera and the Longitudinal Valley. Further west,
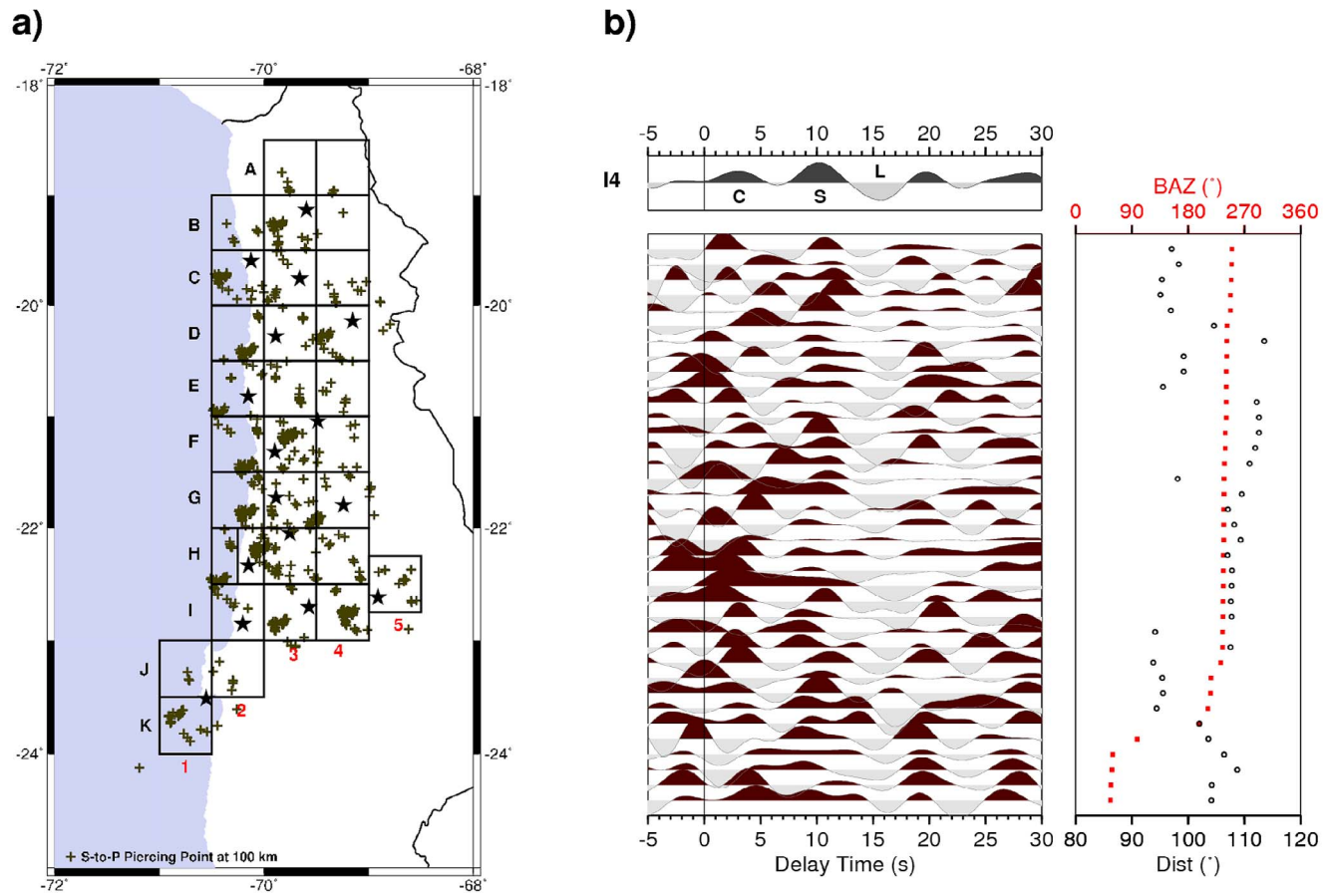
Figure 3. (a) Distribution of the *S*-to-*P* conversion points at 100 km depth. Locations of the seismic stations are shown by black stars. The region has been divided into 31 boxes denoted by letters and numbers. (b) Moveout-corrected SRFs calculated for box I4, located about 80 km away from station PB03. The data are filtered using a low-pass filter of 4 s and sorted by back azimuth. The LAB phase is well resolved at 15 s.

beneath the Coastal Cordillera, this phase is no longer visible and seems to be continued by negative converted phases. Such a reversal of sign for the Moho conversion has been previously observed by *Bostock et al.* [2002] and *Sodoudi et al.* [2006b] beneath the Cascadia and Hellenic subduction zones, respectively. They interpreted the negative Moho phase as a reversed Moho velocity contrast caused by a large amount of serpentinite in the forearc mantle wedge. Another explanation for the absence of the continental Moho phase beneath the Coastal Cordillera could be the strong converted energy of the oceanic Moho, which dominates the receiver functions and masks the continental Moho conversion.

[13] The Moho of the subducting Nazca plate (labeled slab) is significantly imaged throughout the whole profile, at depths ranging from 50 km beneath the Coastal Cordillera to an average of about 80 km beneath the Longitudinal Valley and 110 km beneath the Western Cordillera. The seismicity recorded during the PISCO'94, ANCORP'96 and PUNA'97 (operation time from 3 months to more than 1 year) experiments [see also *Schurr et al.*, 2006] is also consistent with the geometry of the slab. Our results confirm the previous estimates of crustal thickness in the central Andes from seismological observations [e.g., *Beck et al.*, 1996,

Beck and Zandt, 2002; *Yuan et al.*, 2000, 2002] and wide-angle reflections [e.g., *Oncken et al.*, 2003; *Wigger et al.*, 1994] and obtain new detailed information on the crustal thickness beneath the Coastal Cordillera and Longitudinal Valley. *Yuan et al.* [2002] provided a Moho depth map for the central Andes using *P* receiver functions, which complemented the Moho depth estimates previously obtained from wide-angle seismic studies and receiver functions [*Beck et al.*, 1996; *Beck and Zandt*, 2002; *Bock et al.*, 2000; *Wigger et al.*, 1994; *Zandt et al.*, 1996]. However, they could not significantly investigate the Moho depth beneath the Coastal Cordillera and Longitudinal Valley.

[14] The PRF data along the profile at 22°S confirmed the presence of a thick crust (60 km) up to the Longitudinal Valley (Figure 5b). However, the data clearly revealed a relatively lower dip angle for the slab than that observed along latitude 20°S (Figure 5a). The dip of the slab down to a depth of 60 km is similar to that obtained along 20°S, indicating that the seismogenic interplate contact does not show variations in dip along the strike of the trench down as far as depths of 60 km (see also Figure 4b). The significant difference in the dip of the slab can be seen at depths greater than 60 km. At depths between 60 and 90 km, the slab (along the profile at 20°S) becomes steeper (~23°), leading
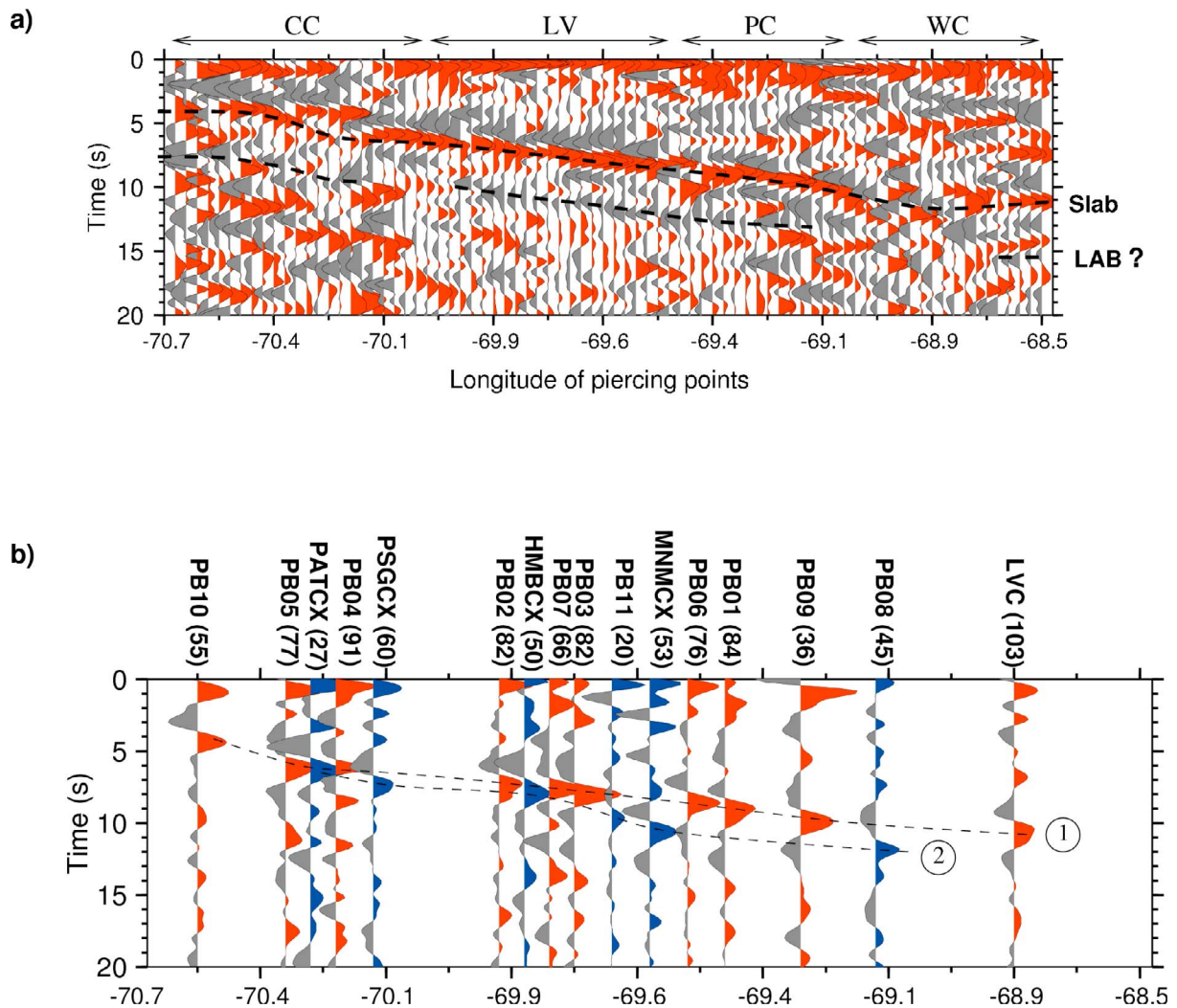
Figure 4. (a) Moveout-corrected *P* receiver functions obtained from all stations and stacked in bins of 0.05 deg and sorted according to the longitude of their piercing points at 100 km depth. The Moho of the downgoing Nazca plate (marked as slab) is observed at times ranging from 4 to 11 s. A negative phase seen in some parts (marked as LAB) of the plot may show some indication of the LAB. (b) Summations of PRFs for all stations sorted by longitude. The number of receiver functions stacked for each station is shown above each trace. The subducting Nazca plate seems to have two different dips (marked as 1 and 2). PRFs obtained from the stations located to the south of 21°S (in red) reveal a significantly lower dip angle (19°) for the Nazca slab compared with that derived from stations to the north of 21°S (in blue). The northern segment of the subducting Nazca plate is steeper (23°) and deeper than the southern segment.

to a depth of about 110 km beneath the Western Cordillera, whereas the slab shows a constant dip angle of about 19° along the profile at 22°S. This variation in the geometry of the subducted plate may support the gradual southward flattening of the slab in northern Chile, as suggested by *Comte and Suárez* [1995]. It should be noted that we have been able to resolve this characteristic more clearly and at a better resolution than other similar studies of northern Chile. The conditions that influence the change in the dip of the slab in northern Chile are still unclear. One possible factor could be variations in curvature of the plate margin. The western margin of South America occurs as a variety of shapes relative to the approaching Nazca plate in northern Chile [*Cahill and Isacks*, 1992]. A major bend in the Chile Trench and in the coastline occurs at exactly 20°S, while the

geological structures (i.e., the trench and coastline) appear to be less complex to the south of this latitude.

[15] The SRFs obtained from the boxes shown in Figure 3a are presented in Figure 6. Beneath all the boxes where the slab phases were reasonably identifiable (labeled S), we also observed the presence of negative phases, which is likely corresponded to the LAB of the oceanic plate. The quality of each summation trace is significantly depended on the number of SRFs located within the corresponded box. We converted times into the depth domain using the reference velocity model of IASP91. The results derived from the boxes to the north of 21°S are shown in Figure 6a. The LAB (labeled L) is seen at a depth of about 80 km beneath the offshore region and at 110 km beneath the Coastal Cordillera, before dipping from 120 km beneath the Longitudinal
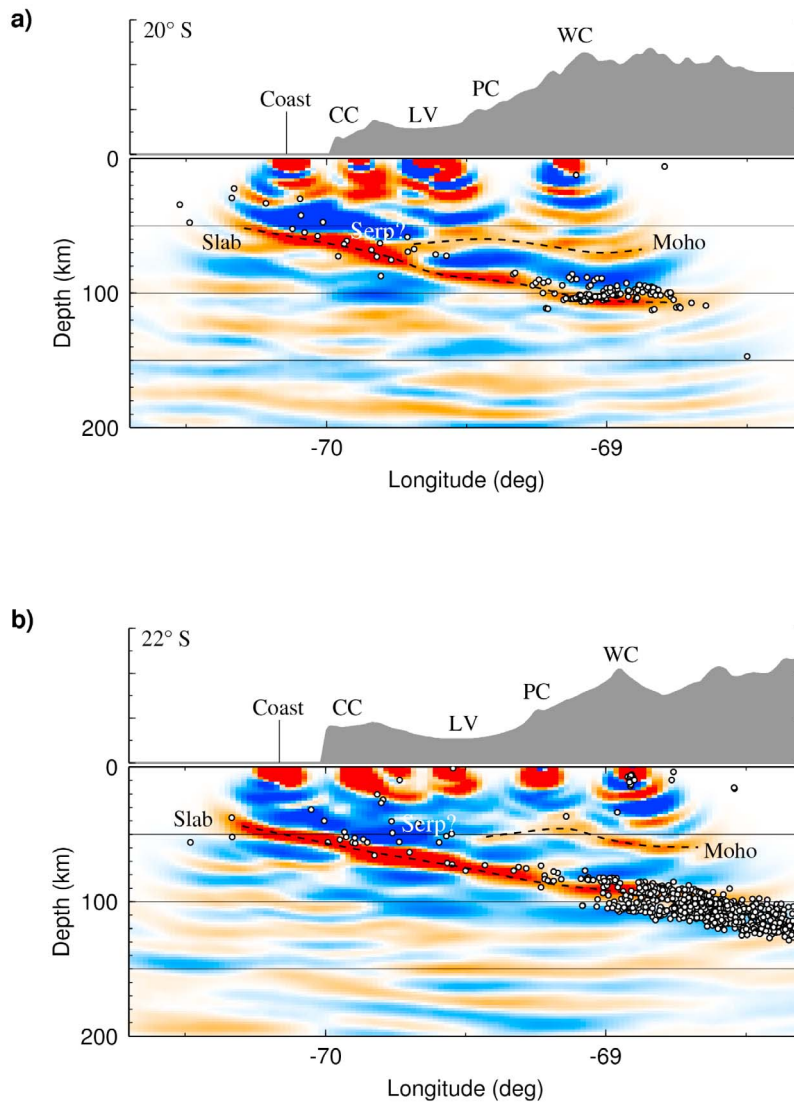
Figure 5. (a) Migrated PRFs along the east-west profile at 20°S. The PRFs obtained from the stations to the north of 21°S are used. Positive (negative) phases are shown in red (blue). The Moho of the continental South American plate (labeled Moho) is well observed at 60–70 km depth beneath the WC, PC, and LV. This phase is not more visible beneath the CC, probably due to serpentinized mantle wedge (labeled serp). The subducted Nazca Moho is indicated down to a depth of 110 km beneath the WC. The black circles are the earthquake hypocenters [*Schurr et al.*, 2006] obtained from other experiments in northern Chile. (b) Same as Figure 5a along an east-west profile at 22°S. Note that the slab is shown deeper and steeper along the profile shown in Figure 5a than that shown in Figure 5b.

Valley to about 150 km under the Western Cordillera. This phase could not be satisfactorily resolved using our migrated PRF data (Figure 5a). SRF analysis for the boxes to the south of 21°S (Figure 6b) reliably indicates the LAB, which occurs slightly shallower than that found beneath the northern part. The geometry of the oceanic Moho (labeled S) obtained from the SRF data is in good agreement with that shown using the PRF data (Figure 5), whereas the long-period SRFs could not resolve the continental Moho (labeled M).

[16]   In order to summarize our results, we show (Figure 7) the section obtained by PRF analysis for the profile at 22°S in time scale. Individual *P* receiver functions are considered in the data bands of 1° at each side of the profile and binned in 0.05°. The SRF data obtained for the same area (Figure 6b) are overlaid on the PRF data (Figure 7a). The correlation obtained between our *P* and *S* receiver functions is significant. The LAB phases, which are reliably resolved by the SRF data, may also be clearly seen beneath the Coastal Cordillera and Longitudinal Valley in the PRF data. Further east (between PC and WC), the correlation between *P* and *S* receiver functions is not better probably due to the small number of SRFs located in the last two boxes (box H4 and G4). Inclusion of high frequencies and consideration of single bin plots in PRF analysis indicate that the phases are distinct from surrounding phases and do not represent side lobes. Therefore, the observed negative phases likely represent direct conversions from sharp velocity drops at associated
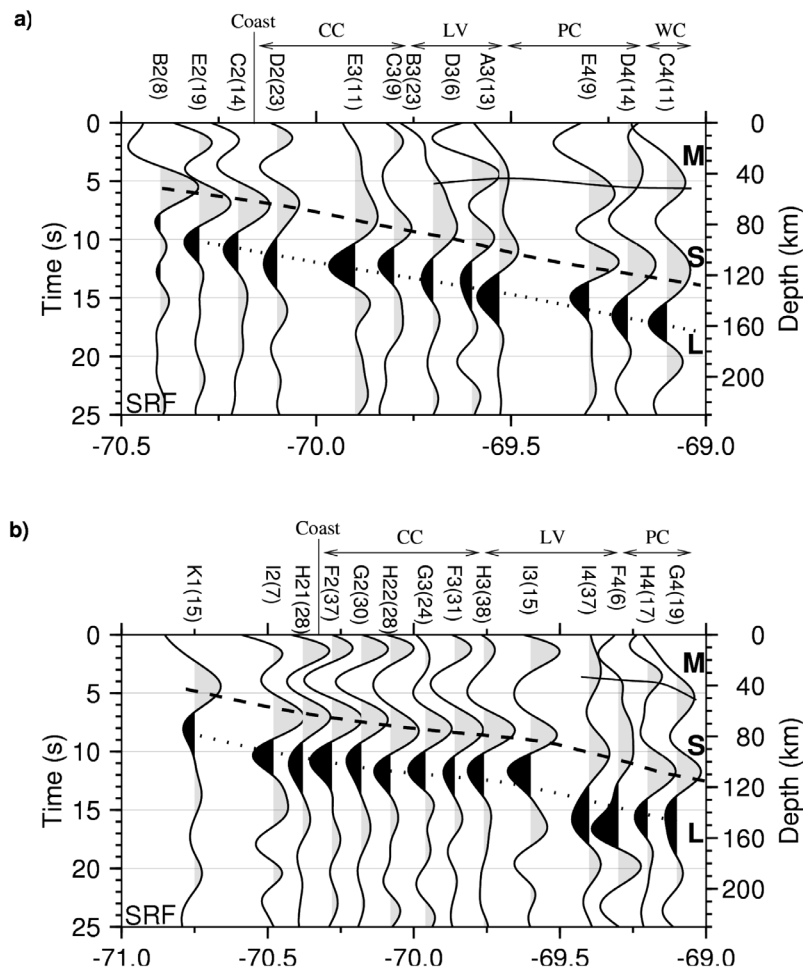
Figure 6. Stacked *S* receiver functions obtained from the boxes shown in Figure 3a and sorted by the longitude of the center of the boxes along the same profiles as shown in Figure 5. Time is converted to depth using the IASP91 reference model. The box numbers and number of SRFs in each box are shown at the top. (a) SRFs obtained from the boxes to the north of 21°S. The slab phase (in black, dashed line, labeled S) is well observed and is in good correlation with our results as shown in Figure 5. The conversion from the LAB (in gray, dotted line, labeled L) is clearly resolved by the SRFs. The continental Moho conversion is not well imaged by SRFs (solid line, labeled M). (b) Same as Figure 6a for the boxes to the south of 21°S.

depths. Previous results in other oceanic regions showed also a sharp LAB (velocity drop of 7–8%) over less than 10–15 km [e.g., *Kawakatsu et al.*, 2009; *Rychert and Shearer*, 2009].

[17] Furthermore, high-resolution PRF data have enabled us to resolve another dominant dipping negative phase 1.3 s earlier than the positive slab phase (Figure 7b), which cannot be interpreted as a side lobe of the *P* signal because it is too large and appears only on one side of the positive phase. We interpreted this phase as the top of the oceanic crust. A low-velocity layer on top of the slab was previously reported in other subduction zones [*Audet et al.*, 2009, 2010; *Ferris et al.*, 2003; *Helffrich and Abers*, 1997; *Kawakatsu et al.*, 2009; *Nikulin et al.*, 2009; *Shiomi and Park*, 2008; *Yuan et al.*, 2000]. *Yuan et al.*, 2000 also found a strong negative phase just before the positive Nazca converter phase in central Andes and showed that a model without a low-velocity layer is unable to explain the large negative signals in front of the positive Nazca converter.

[18] We thus obtain a good estimate of the thickness of the Nazca lithosphere, using reliable arrival data from the top and bottom of the oceanic lithosphere. Beneath the Coastal Cordillera and Longitudinal Valley, the top of the oceanic lithosphere is clearly shown by the PRF data. The results that show the bottom of the lithosphere (the LAB) obtained from the *P* and *S* receiver functions seem also to be consistent beneath this region. The depths derived using the high-frequency PRF data have smaller errors than those obtained using the SRF data. The error introduced into the determination of the depth of the slab as shown by the PRF data is generally less than 5 km. Using our PRF data, the difference between the top and bottom of the Nazca lithosphere is estimated to be about 6 s (Figure 7b), which suggests a lithospheric thickness of about 50 km (±5 km) for the oceanic Nazca plate. Recent work by *Sdrolias and Müller* [2006] showed that the age of the subducting Nazca lithosphere may be assumed to be ~50 My in northern Chile. The thickness and age of the Nazca lithosphere are in good
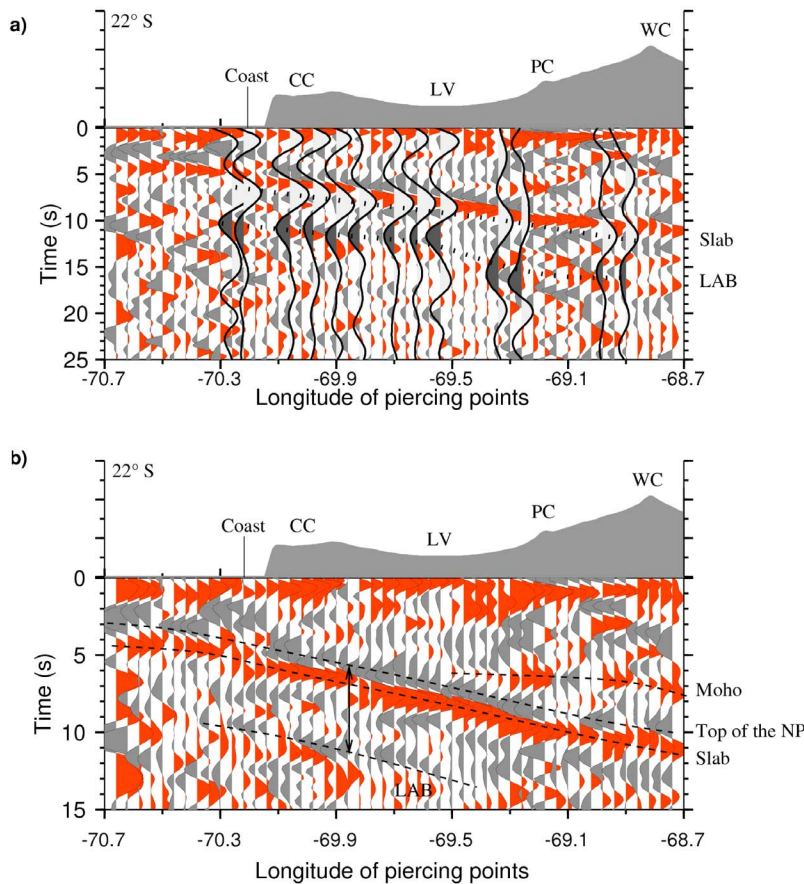
Figure 7. (a) SRFs obtained from the boxes to the south of 21°S (Figure 6a) overlaid on the PRF section. The PRF section has been prepared using binned PRF data (0.05 deg) along the profile at 22°S. The LAB phase resolved by the SRFs is also well observed in the PRF section. (b) Same as Figure 7a without the SRF data. The LAB is clearly resolved beneath the CC and LV using high-frequency PRF data. The top of the Nazca plate (NP) is also clearly visible as a negative phase that occurs just before the slab phase. The thickness of the subducting Nazca lithosphere is clearly indicated by the PRF data (black arrow).

agreement with the thermal gradients (isotherm at 1000°) suggested by *Stein and Stein* [1992]. The thickness of the Nazca lithosphere is thus consistent with the thermally controlled origin for the oceanic LAB. The LAB shown by the PRF data at high frequencies is sharp and cannot be explained by thermal gradients alone, however. A wide variety of recent studies are consistent with an oceanic lithosphere that corresponds to a dry, chemically depleted layer over a hydrated, fertile asthenosphere [*Fischer et al.*, 2010; *Kawakatsu et al.*, 2009; *Rychert and Shearer*, 2009]. In agreement with them we conclude that the observed significant drop in shear wave velocity at the Nazca LAB is probably best explained by a mechanism such as composition, hydration or melting.

5. Conclusions

[19] We analyzed about 3 years of seismic data obtained from 15 IPOC stations in northern Chile for *P*-to-*S* and *S*-to-*P* converted phases. A downgoing interface, correlated with the Moho of the subducting Nazca plate, was clearly seen at depths ranging from 50 km beneath the Coastal Cordillera, to an average depth of 80 km beneath the Longitudinal Valley, and about 110 km beneath the Western

Cordillera. The shape of the Nazca plate shows a low dip angle (19°) to the south of latitude 21°S, but it becomes steeper (23°) and deeper to the north of this latitude. This observation is coherent with the intermediate-depth seismicity and mainly supports the view of a gradual southward flattening of the slab in northern Chile. We attribute the changes in the angle of subduction to the curvature of the plate margin and character of the overriding plate. Our PRF data reliably revealed a thick crust (60–70 km) for the South American plate beneath its eastern section up to the Longitudinal Valley. The serpentinization that occurs in the forearc mantle wedge probably makes the corresponding continental Moho phase invisible beneath the Coastal Cordillera. Using data from our *P* and *S* receiver functions, we found a clear indication of the presence of the LAB beneath the oceanic Nazca plate. The LAB of the subducting Nazca plate was clearly seen as a sharp boundary, which lies at a depth of 80 km beneath the coastal area and dips from a depth of 110 km beneath the Coastal Cordillera to about 150 km underneath the Western Cordillera. High-frequency PRF data enabled us to make confident estimates of the top and bottom of the Nazca lithosphere, which results in a lithospheric thickness of about 50 km. In relation to the age of the Nazca

plate, which is assumed to be ~ 50 My beneath northern Chile, the obtained thickness can be explained by a thermally controlled origin for the oceanic LAB. Furthermore, the existence of S-to-P and P-to-S phases from the Nazca LAB showed that the LAB velocity gradient is relatively sharp. This implies that the LAB probably represents a boundary in terms of hydration and melting, and not in temperature alone.

References

Abt, D. L., K. M. Fischer, S. W. French, H. A. Ford, H. Yuan, and B. Romanowicz (2010), North American lithospheric discontinuity structure imaged by Ps and Sp receiver functions, *J. Geophys. Res.*, *115*, B09301, doi:10.1029/2009JB006914.

Angermann, D., J. Klotz, and C. Reigber (1999), Space-geodetic estimation of the Nazca-South American Euler vector, *Earth Planet. Sci. Lett.*, *171*, 329–334, doi:10.1016/S0012-821X(99)00173-9.

Audet, P., M. G. Bostock, N. I. Christensen, and S. M. Peacock (2009), Seismic evidence for overpressured subducted oceanic crust and megathrust fault sealing, *Nature*, *457*, 76–78, doi:10/1038/nature07650.

Audet, P., M. G. Bostock, D. C. Boyarko, M. R. Brudzinski, and R. M. Allen (2010), Slab morphology in the Cascadia fore arc and its relation to episodic tremor and slip, *J. Geophys. Res.*, *115*, B00A16, doi:10.1029/2008JB006053.

Barazangi, M., and B. L. Isacks (1976), Spatial distribution of earthquakes and subduction of the Nazca plate beneath South America, *Geology*, *4*, 686–692, doi:10.1130/0091-7613(1976)4<686:SDOEAS>2.0.CO;2.

Beck, S. L., and G. Zandt (2002), The nature of orogenic crust in the central Andes, *J. Geophys. Res.*, *107*(B10), 2230, doi:10.1029/2000JB000124.

Beck, S. L., G. Zandt, S. C. Myers, T. C. Wallace, P. G. Silver, and L. Drake (1996), Crustal-thickness variations in the central Andes, *Geology*, *24*, 407–410, doi:10.1130/0091-7613(1996)024<0407:CTVITC>2.3.CO;2.

Bevis, M., and B. L. Isacks (1984), Hypocentral trend surface analysis: Probing the geometry of Benioff zones, *J. Geophys. Res.*, *89*, 6153–6170, doi:10.1029/JB089iB07p06153.

Bock, G., B. Schurr, and G. Asch (2000), High-resolution image of the oceanic Moho in the subducting Nazca plate from P-S converted waves, *Geophys. Res. Lett.*, *27*, 3929–3932, doi:10.1029/2000GL011881.

Bostock, M. G., R. D. Hyndman, S. Rondenay, and A. M. Peacock (2002), An inverted continental Moho and serpentinization of the forearc mantle, *Nature*, *417*, 536–538, doi:10.1038/417536a.

Buske, S., S. Lüth, H. Meyer, R. Patzig, C. Reichert, S. Shapiro, P. Wigger, and M. Yoon (2002), Broad depth range seismic imaging of the subducted Nazca slab, north Chile, *Tectonophysics*, *350*, 273–282, doi:10.1016/S0040-1951(02)00117-8.

Cahill, T., and B. L. Isacks (1992), Seismicity and shape of the subducted Nazca plate, *J. Geophys. Res.*, *97*, 17,503–17,529, doi:10.1029/92JB00493.

Cammarano, F., and B. Romanowicz (2007), Insights into the nature of the transition zone from physically constrained inversion of long-period seismic data, *Proc. Natl. Acad. Sci. U. S. A.*, *104*, 9139–9144, doi:10.1073/pnas.0608075104.

Comte, D., and G. Suárez (1995), Stress distribution and geometry of the subducting Nazca plate in northern Chile using teleseismically recorded earthquakes, *Geophys. J. Int.*, *122*, 419–440, doi:10.1111/j.1365-246X.1995.tb07005.x.

Ferris, A., G. A. Abers, D. H. Christensen, and E. Veenstra (2003), High-resolution image of the suducted Pacific plate beneath central Alaska, 50–150 km depth, *Earth Planet. Sci. Lett.*, *214*, 575–588, doi:10.1016/S0012-821X(03)00403-5.

Fischer, K. M., H. A. Ford, D. L. Abt, and C. A. Rychert (2010), The lithosphere-asthenosphere boundary, *Annu. Rev. Earth Planet. Sci. Lett.*, *38*, 551–575.

Geissler, W. H., F. Sodoudi, and R. Kind (2010), Thickness of the central and eastern European lithosphere as seen by S receiver functions, *Geophys. J. Int.*, *181*, 604–634.

Giese, P., E. Scheuber, F. Schilling, M. Schmitz, and P. Wigger (1999), Crustal thickening processes in the central Andes and the different nat-

ures of the Moho-discontinuity, *J. South Am. Earth Sci.*, *12*, 201–220, doi:10.1016/S0895-9811(99)00014-0.

Götze, H. J., B. Lahmeyer, S. Schmidt, and S. Strunk (1994), The lithospheric structure of the central Andes (20–25°S) as inferred from quantitative interpretation of regional gravity, in *Tectonics of the Southern Central Andes: Structure and Evolution of an Active Continental Margin*, edited by K. Reutter et al., pp. 23–48, Springer, Berlin.

Gurnis, M., C. Hall, and L. Lavier (2004), Evolving force balance during incipient subduction, *Geochem. Geophys. Geosyst.*, *5*, Q07001, doi:10.1029/2003GC000681.

Haberland, C., and A. Rietbrock (2001), Attenuation tomography in the western central Andes: A detailed insight into the structure of a magmatic arc, *J. Geophys. Res.*, *106*, 11,151–11,167, doi:10.1029/2000JB900472.

Heit, B., F. Sodoudi, X. Yuan, M. Bianchi, and R. Kind (2007), An S receiver function analysis of the lithospheric structure in South America, *Geophys. Res. Lett.*, *34*, L14307, doi:10.1029/2007GL030317.

Helffrich, G., and G. A. Abers (1997), Slab low-velocity layer in the eastern Aleutian subduction zone, *Geophys. J. Int.*, *130*, 640–648, doi:10.1111/j.1365-246X.1997.tb01858.x.

Husen, S., E. Kissling, E. Flueh, and G. Asch (1999), Accurate hypocentre determination in the seismogenic zone of the subducting Nazca Plate in northern Chile using a combined on-/offshore network, *Geophys. J. Int.*, *138*, 687–701, doi:10.1046/j.1365-246x.1999.00893.x.

Kawakatsu, H., P. Kumar, Y. Takei, M. Shinohara, T. Kanazawa, E. Araki, and K. Suyehiro (2009), Seismic evidence for sharp lithosphere-asthenosphere boundaries of oceanic plates, *Science*, *324*, 499–502.

Kennett, B. L. N., and E. R. Engdahl (1991), Travel times for global earthquake location and phase identification, *Geophys. J. Int.*, *105*, 429–465, doi:10.1111/j.1365-246X.1991.tb06724.x.

Khazaradze, G., and J. Klotz (2003), Short- and long-term effects of GPS measured crustal deformation rates along the south central Andes, *J. Geophys. Res.*, *108*(B6), 2289, doi:10.1029/2002JB001879.

Kumar, P., X. Yuan, R. Kind, and J. Ni (2006), Imaging the colliding Indian and Asian continental lithospheric plates beneath Tibet, *J. Geophys. Res.*, *111*, B06308, doi:10.1029/2005JB003930.

Kustowski, B., G. Ekström, and A. M. Dziewoński (2008), The shear-wave velocity structure in the upper mantle beneath Eurasia, *Geophys. J. Int.*, *174*, 978–992, doi:10.1111/j.1365-246X.2008.03865.x.

Nikulin, A., V. Levin, and J. Park (2009), Receiver function study of the Cascadia megathrust: Evidence for localized serpentinization, *Geochem. Geophys. Geosyst.*, *10*, Q07004, doi:10.1029/2009GC002376.

Oncken, O., et al. (1999), Seismic reflection image revealing offset of Andean subduction-zone earthquake locations into oceanic mantle, *Nature*, *397*, 341–344, doi:10.1038/16909.

Oncken, O., et al. (2003), Seismic imaging of a convergent continental margin and plateau in the central Andes (Andean Continental Research Project 1996 (ANCORP'96)), *J. Geophys. Res.*, *108*(B7), 2328, doi:10.1029/2002JB001771.

Patzwahl, R., J. Mechie, A. Schulze, and P. Giese (1999), Two-dimensional velocity models of the Nazca plate subduction zone between 19.5°S and 25°S from wide angle seismic measurements during the CINCA95 project, *J. Geophys. Res.*, *104*, 7293–7317, doi:10.1029/1999JB900008.

Rietbrock, A., and C. Haberland (2002), Active faulting of the subducting Nazca Slab: Evidence from local earthquake tomography and high precision hypocenters, paper presented at 62nd Jahrestagung der Deutschen Geophysikalischen Gesellschaft, Hannover, Germany.

Rychert, C., and P. Shearer (2009), A global view of the lithosphere-asthenosphere boundary, *Science*, *324*, 495–498, doi:10.1126/science.1169754.

Schurr, B., G. Asch, A. Rietbrock, C. Trumbull, and C. Haberland (2003), Complex patterns of fluid and melt transport in the central Andean subduction zone revealed by attenuation tomography, *Earth Planet. Sci. Lett.*, *215*, 105–119, doi:10.1016/S0012-821X(03)00441-2.

Schurr, B., A. Rietbrock, G. Asch, R. Kind, and O. Oncken (2006), Evidence for lithospheric detachment in the central Andes from local earthquake tomography, *Tectonophysics*, *415*, 203–223, doi:10.1016/j.tecto.2005.12.007.

Sdrolias, M., and R.D. Müller (2006), Controls on back-arc basin formation, *Geochem. Geophys. Geosyst.*, *7*, Q04016, doi:10.1029/2005GC001090.

Shiomi, K., and J. Park (2008), Structural features of the subducting slab beneath the Kii Peninsula, central Japan: Seismic evidence of slab segmentation, dehydration, and anisotropy, *J. Geophys. Res.*, *113*, B10318, doi:10.1029/2007JB005535.

Sodoudi, F., X. Yuan, Q. Liu, R. Kind, and J. Chen (2006a), Lithospheric thickness beneath the Dabie Shan, central eastern from S receiver functions, *Geophys. J. Int.*, *166*, 1363–1367, doi:10.1111/j.1365-246X.2006.03080.x.

Sodoudi, F., R. Kind, D. Hatzfeld, K. Priestley, W. Hanka, K. Wylegalla, G. Stavrakakis, A. Vafidis, H. P. Harjes, and M. Bohnhoff (2006b), Lith-

ospheric structure of the Aegean obtained from *P* and *S* receiver functions, *J. Geophys. Res.*, *111*, B12307, doi:10.1029/2005JB003932.

Sodoudi, F., X. Yuan, R. Kind, B. Heit, and A. Sadidkhouy (2009), Evidence for a missing crustal root and a thin lithosphere beneath the central Alborz by receiver function studies, *Geophys. J. Int.*, *177*, 733–742, doi:10.1111/j.1365-246X.2009.04115.x.

Stein, C., and S. Stein (1992), A model for the global variation in oceanic depth and heat flow with lithospheric age, *Nature*, *359*, 123–129, doi:10.1038/359123a0.

van der Lee, S., D. James, and P. Silver (2001), Upper mantle *S* velocity structure of western and central South America, *J. Geophys. Res.*, *106*, 30,821–30,834, doi:10.1029/2001JB000338.

Wigger, P., et al. (1994), Variation in the crustal structure of the southern central Andes deduced from seismic refraction investigations, in *Tectonics of the Southern Central Andes: Structure and Evolution of an Active Continental Margin*, edited by K. Reutter et al., pp. 23–48, Springer, Berlin.

Yuan, X., J. Ni, R. Kind, J. Mechie, and E. Sandvol (1997), Lithospheric and upper mantle structure of southern Tibet from a seismological passive source experiment, *J. Geophys. Res.*, *102*, 27,491–27,500, doi:10.1029/97JB02379.

Yuan, X., et al. (2000), Subduction and collision processes in the central Andes constrained by converted seismic phases, *Nature*, *408*, 958–961, doi:10.1038/35050073.

Yuan, X., S. V. Sobolev, and R. Kind (2002), Moho topography in the central Andes and its geodynamic implications, *Earth Planet. Sci. Lett.*, *199*, 389–402, doi:10.1016/S0012-821X(02)00589-7.

Zandt, G., S. L. Beck, S. R. Ruppert, C. J. Ammon, D. Rock, E. Minaya, T. C. Wallace, and P. G. Silver (1996), Anomalous crust of the Bolivian Altiplano, central Andes: Constraints from broadband regional seismic waveforms, *Geophys. Res. Lett.*, *23*, 1159–1162, doi:10.1029/96GL00967.

———————

G. Asch, R. Kind, F. Sodoudi, and X. Yuan, Helmholtz Centre Potsdam, GFZ German Research Centre for Geosciences, Telegrafenberg, D-14473 Potsdam, Germany. (foroug@gfz-potsdam.de)